Local Buckling Criteria of Thin-Walled FRP Circular Cylinders under Compression

Seishi YAMADA*, Nobuhisa YAMAMOTO*, James G.A. CROLL, Phanthong BOUNKHONG***

* Toyohashi University of Technology, Hibarigaoka 1-1, Tempaku-cho, Toyohashi 441-8580, Japan
** Fellow of R A Eng, Professor, University College London, Gower Street, London WC1E 6BT, UK

Cylindrical shell elements may be used as the piers of all-FRP bridges or the seismic retrofit covering of existing reinforced-concrete bridge substructures. An elastic nonlinear Ritz analysis is used to study the buckling behavior of axially loaded imperfect fiber reinforced polymeric cylindrical shells. Extensive parameter studies demonstrate the existence of a well-defined lower bound to buckling loads and the dominance of characteristic incremental deformation modes as this lower bound is approached. It is shown that even for the fiber reinforced polymeric composite shells as well as for the isotropic shell the reduced stiffness method provides reliable estimates of the lower bounds to buckling loads and consequently an important basis for design.

Key Words: Fiber Reinforced Polymer, Cylindrical Shell, Imperfection Sensitivity, Elastic Buckling

1. Introduction

Cylindrical shell elements may be used as the piers of all-FRP bridges or the seismic retrofit covering of existing reinforced-concrete bridge substructures. Also for the design of FRP pipes in trussed bridges, the precise estimation of their structural load-carrying capacity would be required because the demand and necessity for such light weight efficient structures has recently led the bridge engineer to the field of structural optimization and simultaneously to the use of such kind of non-conventional materials. There exists a large activity in the area of material characterization, analysis, fabrication and design of composite structures. In this paper the FRP structural members that are modeled are thin-walled orthotropic cylindrical shells and it is their elastic local shell-type buckling criteria under axial compression forces that are considered. It is well-known that axially compressed cylindrical shells have a buckling behavior which is very sensitive to initial geometric imperfections[1].

At the IUTAM Symposium on buckling collapse, held in London in 1982, a number of papers summarized aspects of the research into shell buckling that had been carried out at Tohoku University[2]. This showed that careful non-linear analysis could reproduce, down to the finest detail, careful observations of the buckling of both spherical and cylindrical shells. Recognizing an opportunity to make good the lack of detailed theoretical validation of the reduced stiffness approach, the third author (J.G.A. Croll), subsequently contacted Professor Noboru Yamaki (who died on 16 February 2004 at the age of 84) with a proposal that some carefully planned joint studies be undertaken. It was arranged that the first author (Seishi Yamada) would come to London in 1985 and spend a year working at UCL. This was the start of a collaboration that has been exceptionally fruitful.

First the collaborated project has been carried out for the pressure buckling of cylindrical shells[3]. It was shown that a classical critical load analysis predicts the upper bound bifurcation pressure with an associated symmetric unstable form of post-buckling behaviour. Increasing levels of imperfection result in non-linear paths that display, at least initially, an effectively 2/3rds power law dependence of buckling loads on the level of imperfection. Incremental displacements at the buckling loads show a gradual erosion of the levels of the contributing membrane energy, eventually resulting in a loss of any maximum load when the incremental membrane energy becomes zero. This lower bound to the maximum loads is observed to be closely predicted by the reduced stiffness reinterpretation of the classical bifurcation analysis.

A second example is drawn from a more recent collaboration[4] seeking to validate the very much more complex

interactions that occur in the axial load buckling of cylinders. A vital extension to the reduced stiffness method, appropriate to the buckling of shells under axial load, had earlier been provided in the work of Batista[5] . This seminal work had demonstrated the existence of an additional stabilizing membrane energy term within the modes of a classical critical load analysis that was responsible for the special characteristics of axial load cylinder buckling. It also allowed the reduced stiffness ideas to be much more directly linked to the earlier analysis of this same problem by both Donnell[6] and Koiter[7]. It was shown that a range of imperfect paths, which, apart from their considerably greater overall reductions in load carrying capacity and evidently greater sensitivity to the levels of very small imperfection, show close similarities with the above case of the pressure loaded cylinder. Again, the classical bifurcation load provides an upper bound and the reduced stiffness extension to this classical critical analysis a lower bound to the imperfection sensitive buckling loads.

Referring to these collaboration and many other shell buckling research works[8-15], the present paper investigates the non-linear buckling behaviour of the FRP composite cylindrical shell having material properties similar to previously studied, by Yamada and Komiya[16,17], as part of an experimental programme on the behavior of columns. From accurate solutions of the nonlinear shell equations it will be demonstrated that for increasing amplitudes of initial imperfections the elastic buckling loads exhibit well defined lower bounds.

2. Nonlinear Buckling Analysis

For an imperfect thin-walled circular cylinder of longitudinal length L, wall-thickness t, and radius R, shown in Fig.1, the change in the total potential energy, consequent upon the application of a uniform axial compression stress of σ, may be written as

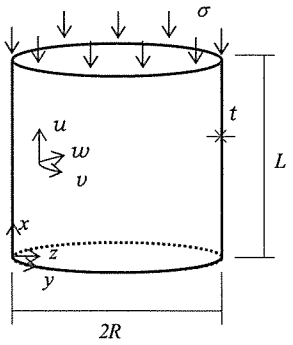

Fig.1 A cylindrical shell

$$\Pi = U_M + U_B + V_\lambda \tag{1}$$

where U_M are the various contribution to the membrane strain energies, U_B the bending energies and V_λ the increase in load potential for an axial compressive stress of σ, are given as

$$U_M = \frac{1}{2}\int_0^{2\pi R}\int_0^{L}\left(n_x\varepsilon_x + n_y\varepsilon_y + 2n_{xy}\varepsilon_{xy}\right)dxdy \tag{2a}$$

$$U_B = \frac{1}{2}\int_0^{2\pi R}\int_0^{L}\left(m_x\kappa_x + m_y\kappa_y + 2m_{xy}\kappa_{xy}\right)dxdy \tag{2b}$$

$$V_\lambda = -\sigma t\int_0^{2\pi R}\int_0^{L}\left(-\frac{\partial u}{\partial x}\right)dxdy \tag{2c}$$

In these expressions, (n_x , n_y , n_{xy}) and (m_x , m_y , m_{xy}) are the total bending and membrane stress resultants, and (ε_x , ε_y , ε_{xy}) and (κ_x , κ_y , κ_{xy}) are the corresponding strains associated with total displacements (u , v , w) from an imperfect but stress-free unloaded state.

The bending and membrane stress resultants are related to strains through the orthotropic constitutive equations

$$n_x = A_{11}\varepsilon_x + A_{12}\varepsilon_y \quad , n_y = A_{12}\varepsilon_x + A_{22}\varepsilon_y \quad , n_{xy} = 2A_{66}\varepsilon_{xy}$$
$$m_x = D_{11}\kappa_x + D_{12}\kappa_y, \; m_y = D_{12}\kappa_x + D_{22}\kappa_y, \; m_{xy} = 2D_{66}\kappa_{xy} \tag{3}$$

The strain-displacement relations associated with deformation from an initial imperfection, w^0 , are taken to be of the Donnell-Mushtari-Vlasov type for shallow shells[6-8] for which

$$\varepsilon_x = \frac{\partial u}{\partial x} + \frac{\partial w^0}{\partial x}\frac{\partial w}{\partial x} + \frac{1}{2}\left(\frac{\partial w}{\partial x}\right)^2 \tag{4a}$$

$$\varepsilon_y = \frac{\partial v}{\partial y} - \frac{w}{R} + \frac{\partial w^0}{\partial y}\frac{\partial w}{\partial y} + \frac{1}{2}\left(\frac{\partial w}{\partial y}\right)^2 \tag{4b}$$

$$\varepsilon_{xy} = \frac{1}{2}\left(\frac{\partial u}{\partial y} + \frac{\partial v}{\partial x} + \frac{\partial w^0}{\partial x}\frac{\partial w}{\partial y} + \frac{\partial w^0}{\partial y}\frac{\partial w}{\partial x} + \frac{\partial w}{\partial x}\frac{\partial w}{\partial y}\right) \tag{4c}$$

$$\kappa_x = -\frac{\partial^2 w}{\partial x^2}, \quad \kappa_y = -\frac{\partial^2 w}{\partial y^2}, \quad \kappa_{xy} = -\frac{\partial^2 w}{\partial x \partial y} \tag{4d}$$

The end boundary is assumed to be supported in such a way as to conform with the classical simple support, corresponding with the conditions.

$$w = 0\ ,\ \frac{\partial w}{\partial x^2} = 0\ ,\ \frac{\partial u}{\partial x} = 0\ ,\ v = 0 \ \text{ at } \ x = 0, L \quad (5)$$

By taking displacement functions u, v and w as linear combinations of the harmonic expressions,

$$u = \sum_i \sum_j^{J_i^u} u_{i,j} \cos(iy/R)\cos(j\pi x/L) \quad (6a)$$

$$v = \sum_i \sum_j^{J_i^v} v_{i,j} \sin(iy/R)\sin(j\pi x/L) \quad (6b)$$

$$w = \sum_i \sum_j^{J_i^w} w_{i,j} \cos(iy/R)\sin(j\pi x/L) \quad (6c)$$

These boundary conditions will be exactly satisfied since each separate component satisfies the boundary conditions of Eq.(6). In these expressions, i and j are the circumferential full-wave and the longitudinal half-wave numbers; $u_{i,j}, v_{i,j}, w_{i,j}$ are the amplitudes of each harmonic function.

The initial geometric imperfection is expressed as

$$w^0 = w^0_{b,f} \cos(by/R)\sin(f\pi x/L) \quad (7)$$

To provide convergence the mode ranges taken in Eq.(7) are for this case adopted as

$$\begin{aligned} J_i^u &= (21,15,11,5) \ \text{ for } \ i = (0,b,2b,3b) \\ J_i^v &= (15,11,5) \quad \text{for } \ i = (b,2b,3b) \\ J_i^w &= (15,11,9) \quad \text{for } \ i = (0,b,2b) \end{aligned} \quad (8)$$

The sets of nonlinear algebraic equations are obtained through the stationary of the total potential energy with respect to each of the displacement degrees of freedom included in Eq.(4). Solution of these sets of nonlinear equations are achieved using a step-by-step process in which either load or displacements are used as control parameter. At each step a Newton-Raphson iteration is used to provide convergence to an acceptable level of precision. A similar description of the theoretical model is included for the isotropic cylinders in Yamada and Croll[3], which lists the integration coefficients for all terms up to and including the quadric energy terms. Appropriate numbers of Newton-Raphson iterations and the choice of a suitable control parameter, depend upon the nature of the local nonlinearities of the equilibrium path[4].

3. Axi-Symmetric Buckling Load and Structural Modeling

For understanding the fundamental local-buckling load-carrying-capacity of orthotropic cylindrical shells, it would be important to obtain the axi-symmetric buckling load which would be associated to the classical buckling load in the case of the isotropic materials. If we substitute i = 0 to Eq.(6), an eigenvalue equation for the linear buckling problem on the basis of the assumption of uniform pre-buckling membrane stress state. Using $(n_x = -\sigma t,\ n_y = 0,\ n_{xy} = 0)$ the axi-symmetric buckling and its associated buckling wave number in the axial direction are now obtained as follows,

$$\sigma_s = \frac{2}{Rt}\sqrt{\left(A_{11}A_{22} - A_{12}^2\right)\frac{D_{11}}{A_{11}}} \quad (9a)$$

$$j_s = \frac{1}{\pi}\sqrt{\frac{L^2}{Rt}}\sqrt{\frac{t^2}{12}\frac{A_{11}A_{22} - A_{12}^2}{D_{11}A_{11}}} \quad (9b)$$

The compressive stress may be written in terms of the non-dimensional load parameter Λ or $\bar{\lambda}$ defined as

$$\Lambda = \sigma/\sigma_s\ , \qquad \bar{\lambda} = \sigma/E_x \quad (10)$$

where E_x is axial Young's modulus which from Eq.(3) can be obtained as follows,

$$E_x = \left(A_{11}A_{22} - A_{12}^2\right)/\left(t\,A_{22}\right) \quad (11)$$

In this analytical study, a commercially available unidirectional glass fiber laminar unit with a 0.2 mm thickness has been adopted and the forty lamination of the unit has used to develop four types orthotropic cylindrical shells with symmetric three-layers and a t = 8mm thickness as listed in Table 1; fiber orientations are relative to the axial direction. Total volume of fiber has been adopted to be V = 60%, and the fiber volume ratio in circumferential direction V_y is adopted to be a parameter in this study. Lamination details are represented in Table 1 and Fig.2. Table 2 shows the coefficients in Eq (4) obtained from the classical lamination theory and coupon test by Yamada and Komiya[16,17].

Table 1 Lamination details

	V_y/V	Laminate configuration
C20T	0.2	90_4 / 0_{32} / 90_4
C50T	0.5	90_{10} / 0_{20} / 90_{10}
C80T	0.8	90_{16} / 0_8 / 90_{16}
C50L	0.5	0_{10} / 90_{20} / 0_{10}

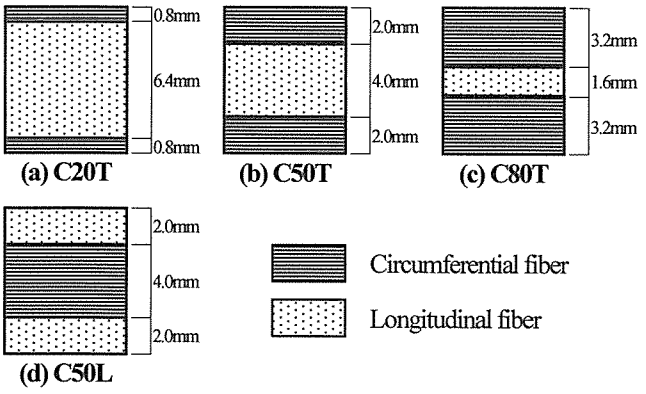

Fig.2 Lamination detail

Table 2 Coefficients in Eqs.(3)-(5)

	A_{11}	A_{12}	A_{22}	A_{66}	D_{11}	D_{12}	D_{22}	D_{66}
	(MN/m)				(N·m)			
C20T	312	14.9	125	23.4	1190	57.2	1150	125
C50T	218	14.9	218	23.4	540	36.4	1780	125
C80T	125	14.9	312	23.4	345	41.6	1970	125
C50L	218	14.9	218	23.4	1780	122	540	125

4. Nature of Buckling

In this paper only the results for shells having $Z = 0.954L^2/(Rt) = 100$ are adopted due to limitness of space. It is well-known that for complete cylinders the geometric Batdorf parameter Z is significant to characteristic classical critical behaviour when the shallow shell assumptions (DMV-formulation) are used. That is, linearized governing equations can be normalized in the terms of the single independent geometric parameter Z. In non-linear postbuckling behaviour, however, the independent geometric parameters are needed. In the present study, the radius thickness ratio R/t has been selected to conform with previous studies[1,3], so that for R/t =405 it follows that L/R=0.512.

Included in Fig.3 are representative imperfect curves for C50T (b=11), where the horizontal axis represents the total displacement component having circumferential wave number b and the single axial wave number, f = 1. It can be seen that the sensitivity of buckling load to changes in imperfection is most severe when the imperfection has a very small amplitude. It is also clear that for moderate large imperfections the buckling loads have induced sensitivity to change in imperfection amplitude, and eventually reach a clear lower bound.

Selected buckling loads Λ^N, obtained from the nonlinear analytical solution, are plotted in Fig.4 for various imperfection amplitudes at different circumferential wave number, b, of the imperfection. The minimum buckling loads Λ^N_{cm} on each figure in Fig.4 are listed in Table 3.

Figure 5 shows the examples of incremental displacement modes at the buckling points for the imperfection mode, b=9. In a shell with relatively large imperfection amplitudes, for example w^0/t=1.60 in Fig.5(b), the same wave number as the adopted imperfection wave number, b=9, dominates. On the other hand, in small imperfection level, the intrinsical buckling modes dominates, and a $2\times b$ number in circumferential direction as shown in Fig.5(b) is clearly seen in this case.

Table 3 Lower limits for non-linear buckling

	Λ^N_{cm}	b (bL/R)	$w^0_{b,1}/t$
C20T	0.230	11 (5.63)	1.20
C50T	0.247	11 (5.63)	1.40
C80T	0.216	9 (4.61)	2.00
C50L	0.131	13 (6.65)	0.80

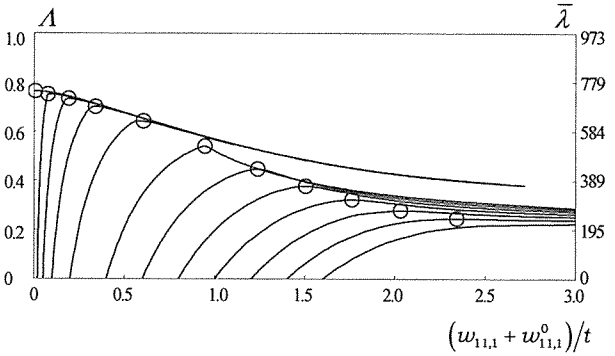

Fig.3 Load versus deflection curves for C50T with b = 11

5. The Lower Boundedness and the Reduced Stiffness Method

The classical bifurcation analysis for a prospective buckling deformation $i = i^c$, $j = j^c$ from a uniform prebuckling stress and strain state could be represented in terms of energy as

$$U_{2B} + U_{2M} + \Lambda^C\left(\frac{\partial V^x_{2M}}{\partial \Lambda} + \frac{\partial V^y_{2M}}{\partial \Lambda}\right) = 0 \qquad (12)$$

In this equation, U_{2B} is the linear bending energy, U_{2M} the linear membrane energy, V^x_{2M} the linearized membrane component associated with axial direction, while V^y_{2M} is associated with circumferential direction. Here "linear" is

in the sense of being related to the linear strain-displacement relationships in the incremental critical deformations. Solution of Eq.(12) will result in the spectra Λ^c of Fig.4. As in Ref.3 i_{cm} is defined to be the circumferential full-wave number associated with the lowest classical linear critical loads.

For the C50T shell, Fig.6 show the breakdown of the total potential energy, where the energies are normalized by $24\pi DL/R$. It can be seen that V_{2M}^x provides the negative destabilizing contributions to the critical loads Λ^c. Both the linear bending U_{2B} and membrane U_{2M} energies contribute to the stabilization, as does the linearized circumferential component V_{2M}^y. In Ref.3 it has been demonstrated that both the linear membrane, U_{2M}, and linearized circumferential, V_{2M}^y, energies are with increasing imperfection eventually eliminated at buckling. Based upon a reduced energy, the critical load, Λ^*, may be obtained by solving the equation for the prospective buckling deformation $i = i^*$ and $j = j^*$, as follows

$$U_{2B} + \Lambda^* \frac{\partial V_{2M}^x}{\partial \Lambda} = 0 \tag{13}$$

This equation gives a simple expression for RS criterion,

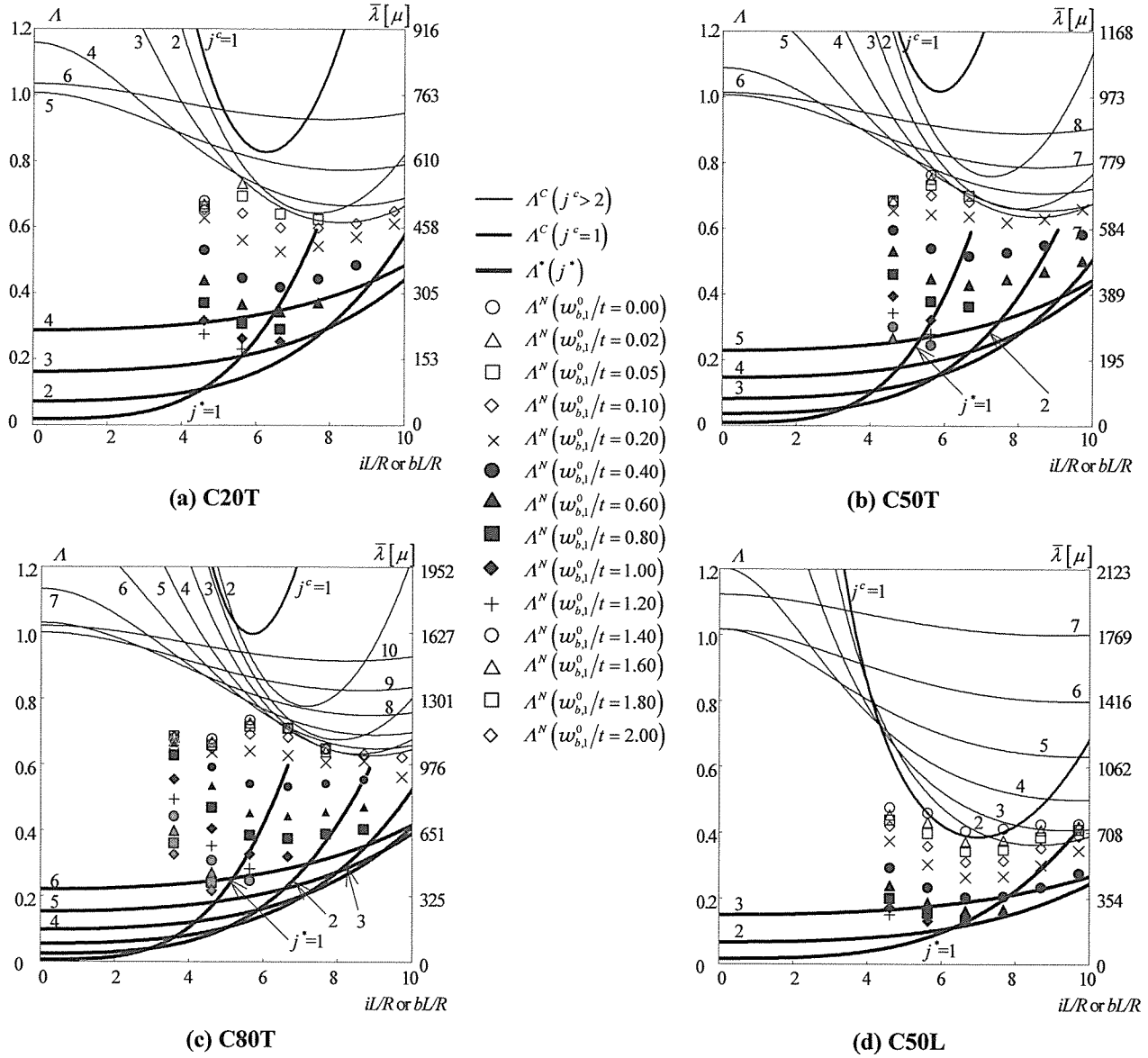

Fig.4 Plots of nonlinear buckling loads for various imperfection amplitudes and circumferential wave number *b* with single axial number compared with the linear buckling loads or the reduced stiffness buckling loads

$$\Lambda^* = \frac{R}{L^2}\sqrt{\left(A_{11}A_{22}-A_{12}^2\right)\frac{A_{11}}{D_{11}}}$$
$$\times\frac{D_{11}(j^*\pi)^4+2(D_{12}+D_{66})(j^*\pi)^2(i^*L/R)^2+D_{22}(i^*L/R)^4}{(2A_{11}A_{22}-A_{12}^2)(j^*\pi)^2+A_{12}A_{22}(i^*L/R)^2} \quad (14)$$

Using Eq.(14), the various reduced stiffness spectrum curves for i^* and j^* can be obtained as shown in the solid curves in Fig.4.

To provide additional confirmation of the lower boundedness of the present reduced stiffness critical load Λ^*, the lower limits of the non-linear analytical buckling loads plotted by various dots in Fig.4 have been compared with the present reduced stiffness analytical results. The many dots in Fig.4, for example, show the buckling loads for imperfections in modes $7 \le b \le 19$ ($3.58 \le bL/R \le 9.73$) and f =1. Those shown for b=13 ($bL/R = 6.65$) relate to the results described in Fig.4(d). For this shell the integer mode nearest to that resulting in the minimum critical load for j=1 is i=13 ($iL/R = 6.65$).

It is evident that the imperfection sensitivity in this mode is at its highest; an imperfection of 80 percent the shell thickness is enough to almost reach the reduced stiffness load.

Figure 7 shows the variation of the linear buckling and reduced stiffness criteria with the circumferential fiber volume V_y/V. The reduced stiffness analytical results $\sigma^*_{cm,j}$ are defined as the minimum reduced stiffness load for axial wave number j; σ^*_{cm} is the minimum of $\sigma^*_{cm,j}$. It can be seen that the circumferential wave number associated with σ^c_{cm}, σ^*_{cm} increases as the ratio V_y/V increase. The maximum of. σ^c_{cm} is obtained when V_y/V = 0.15 for T-series and V_y/V = 0.80 for L-series. Shown in Fig.7 are that σ^*_{cm} is almost constant and the lower bound for design maybe independently determined with the ratio V_y/V.

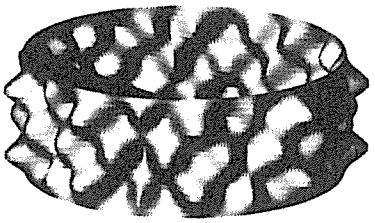

(a) C50T (b=9, w^0/t = 0.10)

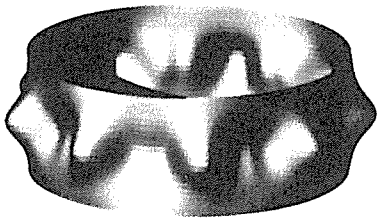

(b) C50T (b=9, w^0/t = 1.60)

Fig.5 Incremental displacement modes at the buckling points

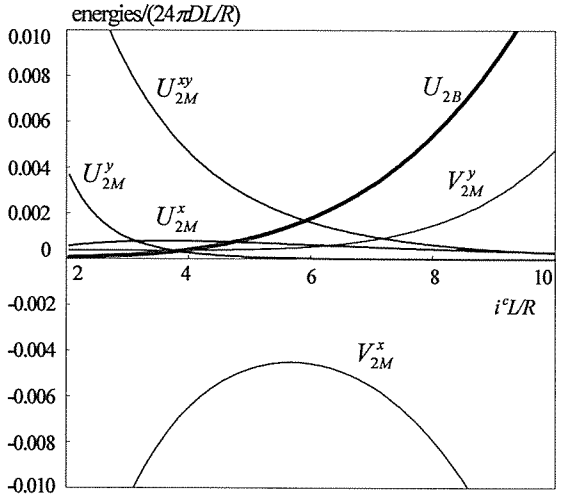

(a) C50T for j^c=1

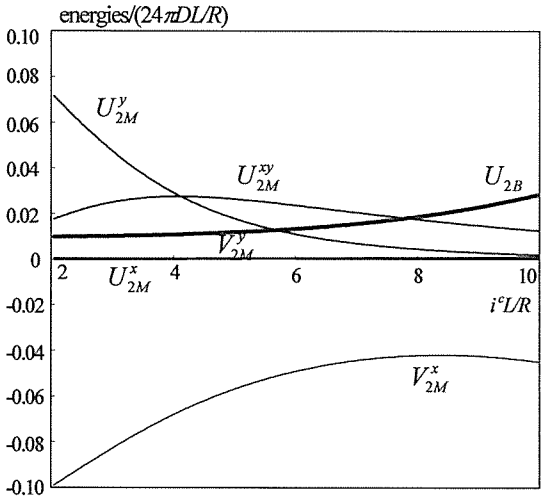

(b) C50T for j^c=4

Fig.6 Energy Components

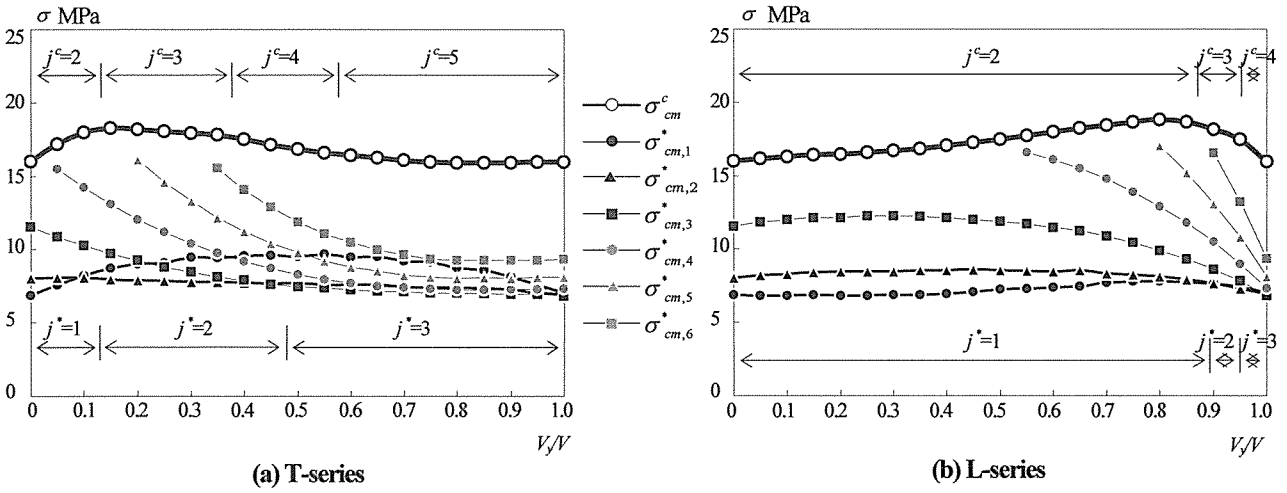

Fig.7 Effects of the ratio V_y/V on the buckling loads

6. Conclusions

In the present study an elastic nonlinear Ritz analysis has been developed to allow investigation of the imperfect behavior of axially compressed orthotropic cylindrical shells. Its buckling loads and modes are strongly influenced by the constitutive material coefficients and are sensitive to initial geometric imperfections. Just as for the previously analysed isotropic cylindrical shells, the reduced stiffness criteria are shown to provide lower bounds to imperfection sensitive elastic buckling loads for orthotropic cylindrical shells. The benefits of the use of the reduced stiffness theoretical results for the optimal design of this kind of complicated composite structures, are in this paper illustrated through the determination of the volume of circumferential fiber instillation volume ratio in detail.

References

1) Yamaki, N.: *Elastic Stability of Circular Cylindrical Shells*, North-Holland, 1984
2) Yamada, M. and Yamada, S.: Agreement between theory and experiment on large-deflection behaviour of clamped spherical shells under external pressure, *Collapse: the Buckling of Structures in Theory and Practice*, Cambridge University Press, pp.431-442, 1983
3) Yamada, S. and Croll, J.G.A.: Buckling and postbuckling characteristics of pressure loaded cylinders, *J. Appl. Mech.*, ASME, Vol.60, pp.290-299, 1993.
4) Yamada, S and Croll, J.G.A.: Contributions to understanding the behavior of axially compressed cylinders, *J Appl. Mech.*, ASME, Vol.66, pp.299-309, 1999.
5) Batista, R.C.: *Lower Bound Estimates for Cylindrical Shell Buckling*, PhD Thesis, University of London, 1979.
6) Donnell, L.H.: A new theory for the buckling of cylinders under axial compression and bending, *Trans. ASME*, Vol.56, p.795, 1934..
7) Koiter, W.T.: *The Effects of Axisymmetric Imperfections on the Buckling of Cylindrical Shells under Axial Compression.* Published in English (1963) as TR-6-90-63-86, Lockhead Missile and Space Co., 1945.
8) Kobayashi, S., Koyama, K., Seko, H. and Hirose, K.: Compressive buckling of graphite-epoxy composite circular cylindrical shells, *ICCM-IV*, pp.555-564, 1982.
9) Dong, S.B. and Etitum, P.: Three-dimensional stability analysis of laminated anisotropic circular cylinders, *Int. J. Solid Struct.*, Vol.32, p.1211, 1995.
10) Croll, J.G.A. and Chilver, A.H.: Approximate estimation of the stability of cooling towers under wind loading, *Proc. IASS Recommendations for the Structural Design of Hyperbolic or Other Similarly Shaped Cooling Towers*, 1971.
11) Croll, J.G.A.: Lower bound elasto-plastic buckling of cylinders, *Proc. Instn Civ. Engrs*, Part 2, Vol.71, pp.235-261, 1981.
12) Yamada, S. and Croll, J.G.A.: Buckling behavior of pressure loaded cylindrical panels, *J. Engrg Mech.*, ASCE, Vol.115, pp.327-344, 1989.
13) Tennyson, R.C. and Hansen, J.S.: Optimum design

for buckling of laminated cylinders, *Collapse: the Buckling of Structures in Theory and Practice*, Cambridge University Press, pp.409-429, 1983.

14) Arbocz, J. and Babcock, C.D.: The effect of general imperfections on the buckling of cylindrical shells, *J. Appl. Mech.*, ASME, Vol.36, pp.28-38, 1969.
15) Batista, R.C. and Croll, J.G.A.: A design approach for axially compressed unstiffened cylinders, *Stability Problems in Engineering Structures and Components*, Applied Science, pp.377-399, 1979.
16) Yamada, S. and Komiya, I.: Elastic deflection behavior of a box-shaped pultruded composite member and its collapse, *Fiber Composites in Infrastructure, ICCI'96*, Tucson, pp.699-707, 1996.
17) Yamada, S., Takashima, H., Tadaka, R. and Komiya, I.: Experiments on the buckling and collapse of pultruded composite columns under axial compression, *Fiber Composites in Infrastructure*, ICCI'98, Arizona, Tucson, Vol.2, pp.236-247, 1998.